SPE 151597

Measurements of Hydraulic-Fracture-Induced Seismicity in Gas Shales

N. R. Warpinski, J. Du, and U. Zimmer, Pinnacle—A Halliburton Service

This paper was prepared for presentation at the SPE Hydraulic Fracturing Technology Conference held in The Woodlands, Texas, USA, 6–8 February 2012.

Abstract

Hydraulic fracturing is an essential technology for hydrocarbon extraction from both conventional and unconventional reservoirs. Recently, concern has developed regarding induced seismicity generated in association with multistage fracturing of horizontal wells in shale reservoirs. A review of thousands of fracture treatments that have been microseismically monitored shows that the induced seismicity associated with hydraulic fracturing is very small and not a problem under any normal circumstances. Results are presented for six major shale basins in North America.

Introduction

Hydraulic fracturing is an important technology for the extraction of hydrocarbons from many reservoirs throughout the world. In unconventional reservoirs, such as the ultralow-permeability shales that are now being regularly exploited, it is absolutely essential to hydraulically fracture a well to obtain economic levels of production (Sutton et al. 2010).

Contrary to media and general public perception, hydraulic fracturing is not a "new" technology, having been applied since the late 1940s (Montgomery and Smith 2010). There is also a perception that hydraulic fractures are much larger than ever, but the "massive hydraulic fractures" that were performed in the 1970s (Fast et al. 1977; Gidley et al. 1979; Strubhar et al. 1980) were of similar size to the fracture treatments that are conducted in horizontal wells today. In addition, these large treatments were performed in shales in the eastern United States (Jennings et al. 1977), with much of the work supported by the United States government (Overby 1978; Duda et al. 2002) to prove up the resources in the Devonian shales of Appalachia and the western tight-gas sandstones of the Rocky Mountains.

A previous paper (Fisher and Warpinski 2011) presented data from microseismic monitoring that showed fractures are not a threat to propagate into aquifers. Results from thousands of monitored fractured treatments demonstrate that fractures will not propagate thousands of feet vertically and intersect potable water sources. In all of the shale basins studied, fractures remain several thousand feet below the deepest aquifer. Hydraulic fracturing is a safe technology as applied in these shale basins.

Recently, however, there has been considerable attention focused on earthquakes associated with hydraulic fracturing. Here, as well, microseismic monitoring is a valuable technology for assessing the earthquake potential of fracturing operations. The objective of this paper is to present the very large suite of microseismic measurements available to the authors in the major shale basins of North America that show that earthquakes are not a threat in any normal situation.

Injection Geomechanics

It is well-understood that long-term injection of fluids in the deep subsurface can induce earthquakes in some circumstances. Nicholson and Wesson (1990) documented numerous cases of minor earthquakes that were likely induced by local injection operations, the most notable of which was the US Army's injection of chemical waste into a 12,000-ft deep interval at the Rocky Mountain Arsenal in Colorado in the 1960s. Similarly, geothermal injections are potential sources of induced seismicity (Fehler 1989; Majer 2005; Smith et al. 2000), often because the optimal geothermal sites are in areas where faults and tectonics are likely to be conducive to earth movement. Other long-term injection operations, such as solution mining, water disposal (Ake et al. 2005), and waterfloods, are potential sources in areas where the geologic conditions are favorable (Segall 1989; Zoback and Harjes 1997).

Simplistically, faults are "locked" because of frictional forces that are primarily a result of the in situ stresses pressing on the fault plane. When the shear stress becomes great enough to overcome the friction, the fault can slip, resulting in an earthquake. Alternately, fluid injection can increase the pore pressure, which acts to neutralize the normal stress on the fault and cause a decrease in the frictional force, again allowing the fault or some other plane of weakness to slip.

Almost any injection process causes some slippage along weakness planes in the earth, but most of these are minuscule, as will be discussed later. Nevertheless, these minuscule earthquakes, termed microseisms, can be very useful for monitoring injection processes, and a relatively significant service industry has developed to apply such technology for industrial processes. The technology for doing this is called microseismic monitoring.

Microseismic Monitoring

Microseismic monitoring is a well-established technology for monitoring hydraulic fractures (Warpinski 2009). It is performed by placing arrays of seismic receivers in offset wellbores that can detect any microearthquakes occurring as a result of the change in stress or pressure induced by the fracturing treatment. There are many important issues that must be adequately addressed to monitor a treatment successfully, the most important of which are location of the monitoring array, determination of an adequate velocity structure, and management of noise. When a test is properly designed and noise is relatively low, microseisms can be detected several thousand feet from the monitoring array, and these microseisms can be located by determining arrivals and polarization of the induced compressional and shear waves. Because the microseisms are located relatively close to the hydraulic fractures (stress effects decay rapidly), this technology can be used to monitor fracture geometry and growth behavior.

In addition to microseismic locations, the actual waveforms contain embedded information about the rock motion. By using standard earthquake seismological principles, it is straightforward to determine the same characteristics of a microseism that would normally be obtained for an earthquake detected by a seismic network. Access to such information provides important data about the actual induced seismicity that occurs as a result of hydraulic fracturing.

Moment, Magnitude, and Size

The definitions of the moment and magnitude of an earthquake, which also apply to a microseism, can be found in any standard textbook on seismology (Aki and Richards 2009). The seismic moment is an applicable measure of the strength of the motion and is given by

$$M_o = \mu d A \quad \text{.....(1)}$$

where μ is the shear modulus of the rock, d is the distance that the fault plane slips, and A is the area of the slippage. For typical shale formations, μ will be on the order of 2.2×10^6 psi (~15 GPa).

The seismic moment has units of ft-lbf, which is the same as energy units, but the energy released by a slippage is typically calculated (Kanamori 1977) as

$$E \approx M_o / 20{,}000 \quad \text{.....(2)}$$

Because both energy and moment span many orders of magnitude, it is usually more convenient to use a log scale, the moment magnitude, which is similar to the Richter magnitude with which most people are familiar. The moment magnitude is given as

$$M_w = \frac{2}{3}\{\log(M_o) - 16.1\} = \frac{2}{3}\{\log E - 11.8\} \quad \text{.....(3)}$$

where the units for this equation are dyne-cm for both M_o and E (M_w is unitless). For conventional oil field units of ft-lbf, the equations become

$$M_w = \frac{2}{3}\{\log(M_o) - 9.0\} = \frac{2}{3}\{\log E - 4.7\} \quad \text{.....(4)}$$

For perspective, an earthquake that can be felt at the surface will have a magnitude of roughly +3, which translates into a moment of 3×10^{13} ft-lbf and energy of 1.5×10^9 ft-lbf. A typical large microseism, with a magnitude of -2, has a moment of ~1.0×10^6 ft-lbf and an energy of ~50 ft-lbf, equivalent to the total work in lifting a 10-lbm weight 5 ft off the ground. It is also important to note that, because of the 2/3 factor in the magnitude equation, the energy increases a factor of 32 for every increase of one magnitude unit.

Results

Fig. 1 shows a plot of the maximum microseismic magnitude for all monitored fracture stages in the Barnett shale up to mid 2011 (within the authors' dataset) as a function of depth. The method for estimating the magnitude, based on an analysis by Brune (1970), is given in a later section. There are thousands of fracturing stages that have been microseismically monitored,

and a wide variance exists in the maximum magnitude. Much of this variance is caused by the geologic setting (e.g., presence of faults, natural fractures, structure), the thickness of the zone, the stress conditions in the reservoir in different locations, the treatment and completion variables, and operational issues. In general, the magnitudes are below +1 M_w, and all of the largest microseisms occur in the deepest part of the reservoir. There is a clear trend of decreasing magnitude with decreasing depth, suggesting that the size of the microseisms is related to the stress conditions in the reservoir. Some of the nearly horizontal patterns are caused by fault interactions because there are many small displacement faults throughout the Barnett shale, and these are easily activated by the fracturing process. However, none of these fault magnitudes approach a size that would remotely be considered problematic. The left-hand border of the data ensemble is indicative of the typical size of microseisms that occur in these reservoirs (<-2.5 M_w), and there are many hundreds or thousands of microseisms that were generated that have these very small magnitudes.

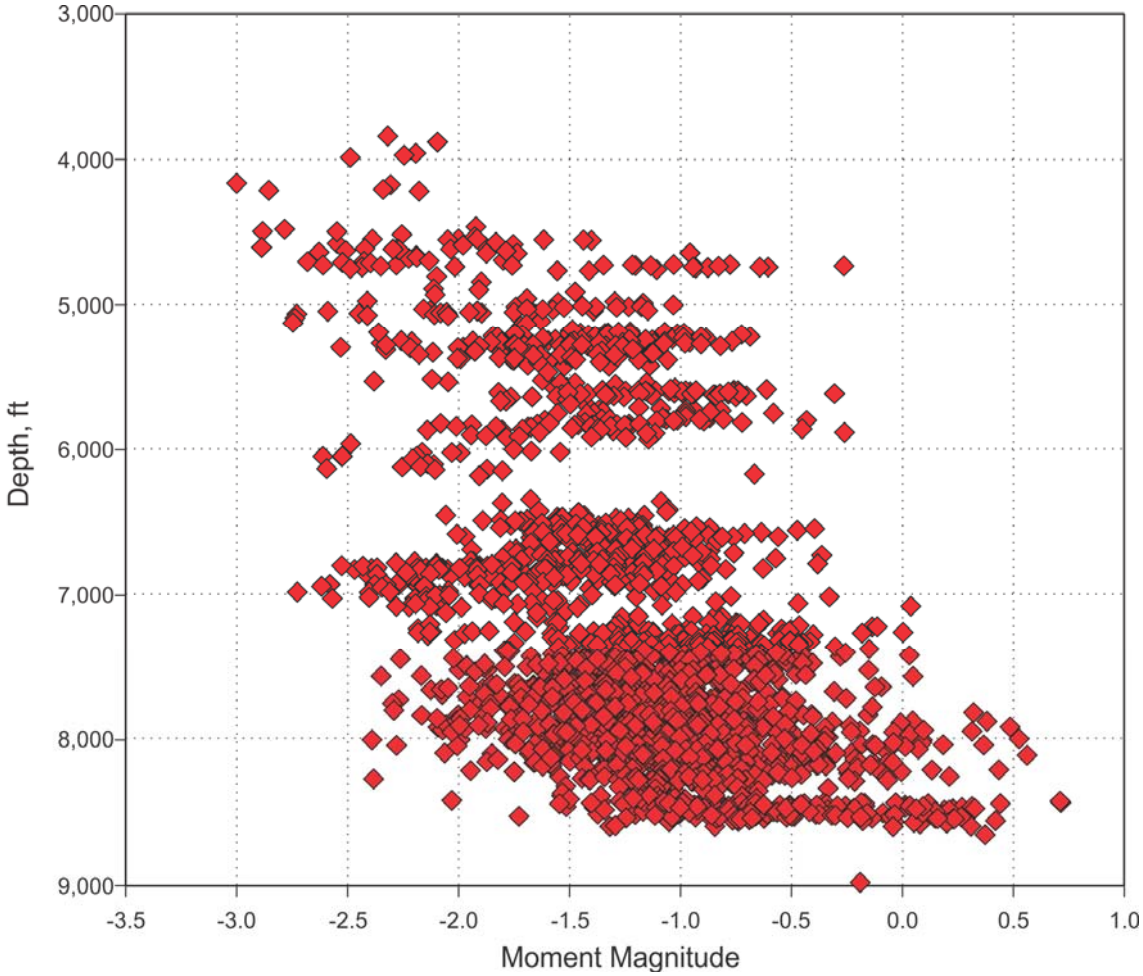

Fig. 1—Barnett shale maximum moment magnitude results for monitored stages through mid 2011.

Fig. 2 shows a similar plot for the Marcellus shale. There are not nearly as many fracture stages that have been monitored in the Marcellus shale as there are in the Barnett shale, but there is a large enough population to clearly show the trends. The most obvious difference is the much smaller maximum magnitude microseisms that are observed in the Marcellus shale. The largest event recorded there to date is smaller than a -0.5 M_w, which is greater than one magnitude unit smaller than the largest microseisms in the Barnett shale. In this basin, the depth effect is not as pronounced, but there is also a smaller depth range. In addition, the span of magnitudes at any depth is considerably less than what is observed in the Barnett shale. In both cases, the typical magnitude is fairly similar, with the smallest maximum magnitudes in the Marcellus shale also being about -2.5 M_w.

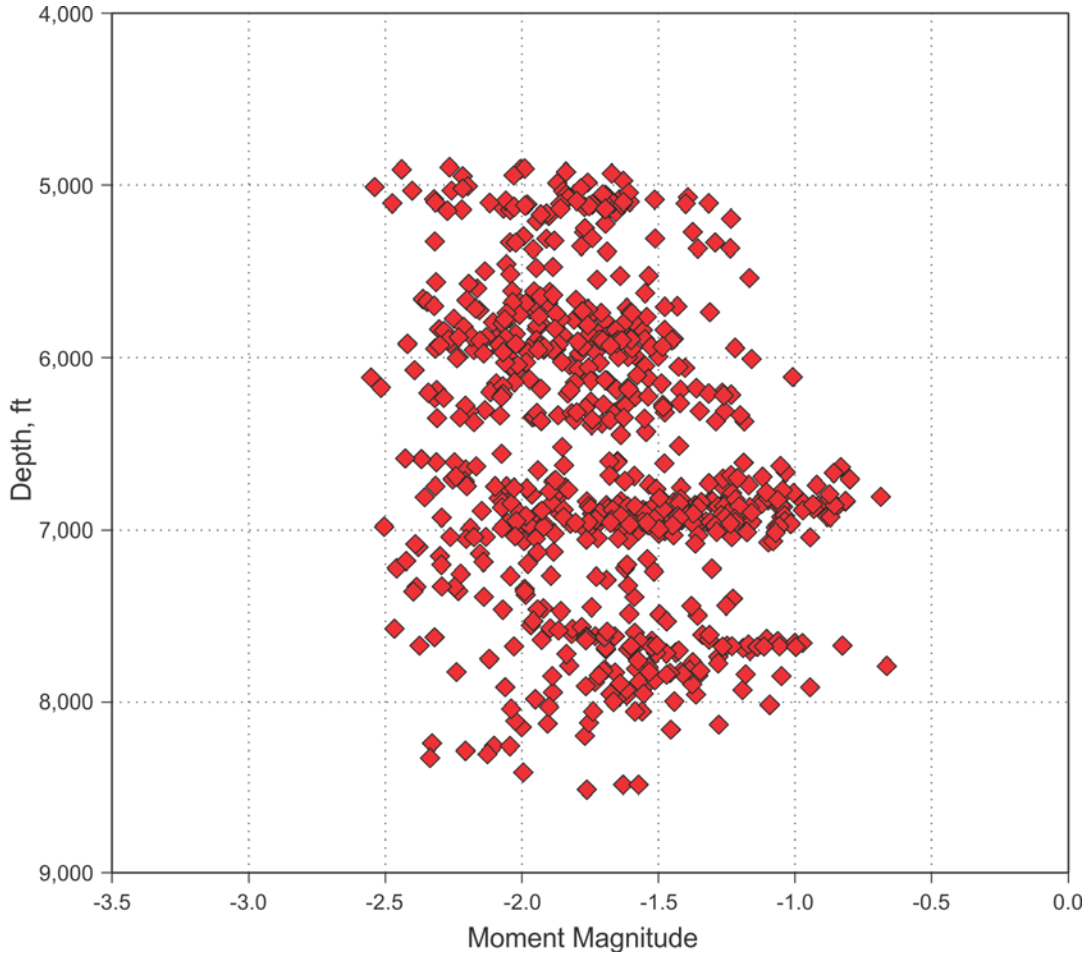

Fig. 2—Marcellus shale maximum moment magnitude results for monitored stages through mid 2011.

Fig. 3 shows similar data for the Eagle Ford formation in south Texas. Much of the work in the Eagle Ford formation is in the liquids-rich section of the play, and no attempt has been made to separate out the data from gas wells relative to those that are primarily oil wells. The maximum magnitude event observed in the Eagle Ford formation through mid 2011 is just below 0 M_w. There is a good correlation between the depth and the maximum magnitude, as in the Barnett shale, but with a much larger depth range. The range of magnitudes is considerably less than the Barnett shale; but, like both the Barnett and the Marcellus shales, the typical event size also appears to be ~ -2.5 M_w. Although there are many faults in the Eagle Ford formation, as clearly delineated in seismic and well construction, there does not appear to be any significant effect on the magnitude of the events.

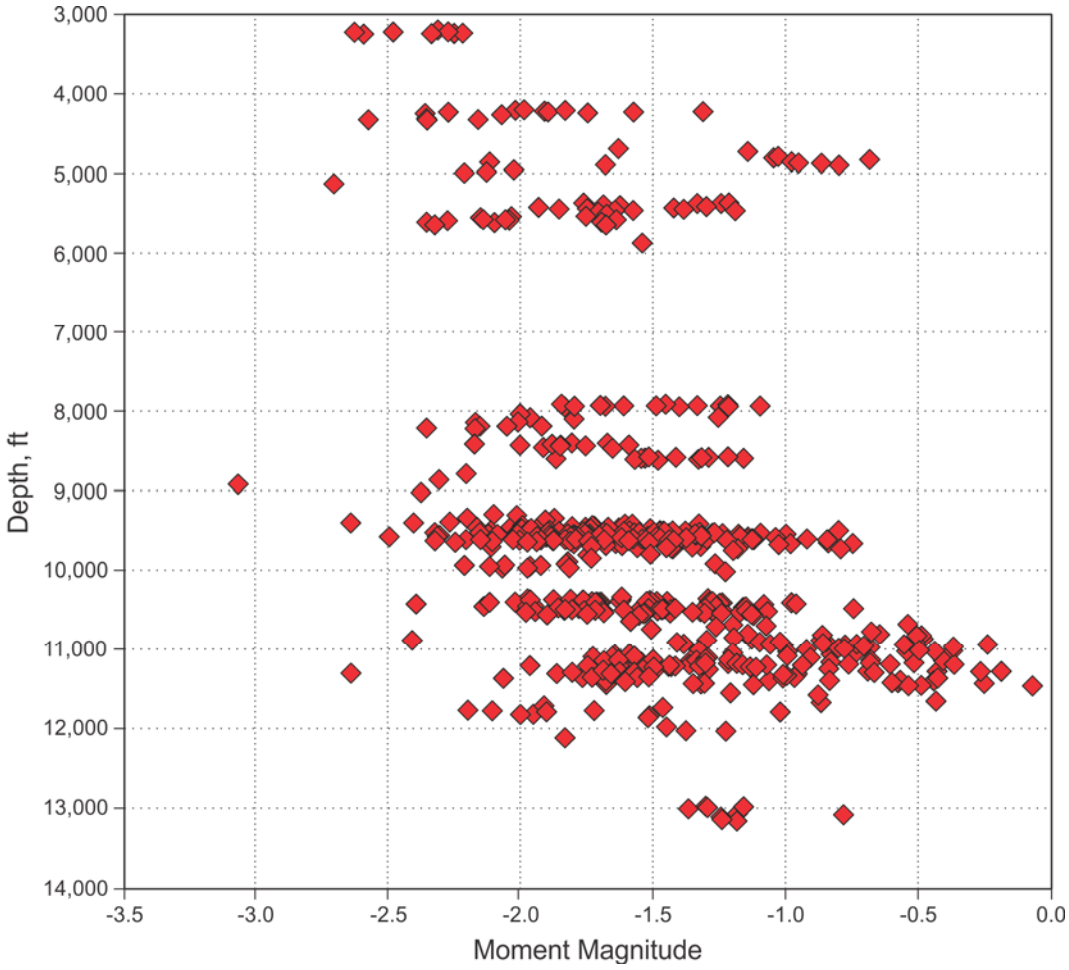

Fig. 3—Eagle Ford formation maximum moment magnitude results for monitored stages through mid 2011.

Data from the Woodford shale are shown in **Fig. 4.** Although somewhat sparser than data sets from the previous three basins, the same types of trends and behavior are obvious. The largest event observed is a little less than 0 M_w, and this happened where the Woodford is considerably deep. Shallow fractures in the Woodford generate relatively low microseismic magnitudes. The spread of the data in Fig. 4 is quite wide, possibly related to the wide depth range, but likely also a result of the complexity of the reservoir, particularly with respect to faults, structure, and dipping beds. Like the other shale reservoirs, a typical microseism would be less than -2 M_w or -2.5 M_w.

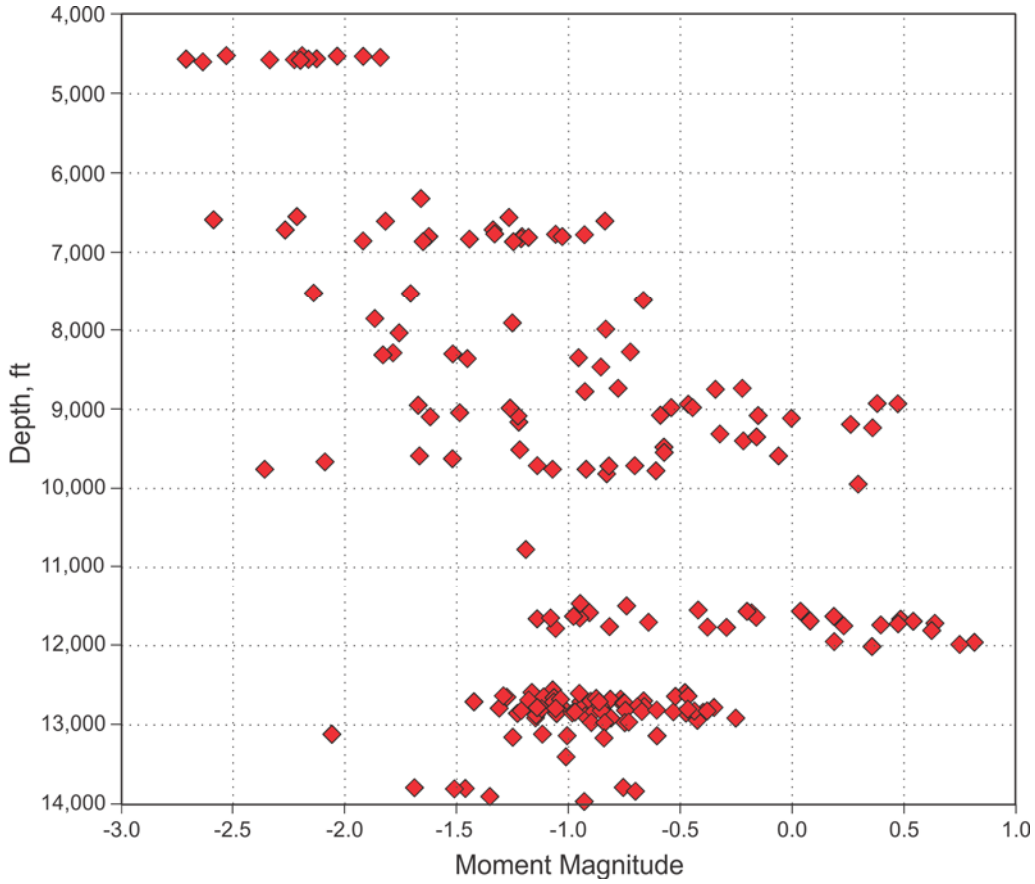

Fig. 4—Woodford shale maximum moment magnitude results for monitored stages through mid 2011.

Data from the Haynesville shale are given in **Fig. 5.** There has been a smaller number of monitored stimulations in the Haynesville shale, at least partly because of current temperature limitations of the receivers. However, of those available, the same trends are present as seen in the other basins. The major difference is the relatively larger magnitudes on the low end, as these are typically on the order of -1.5 M_w.

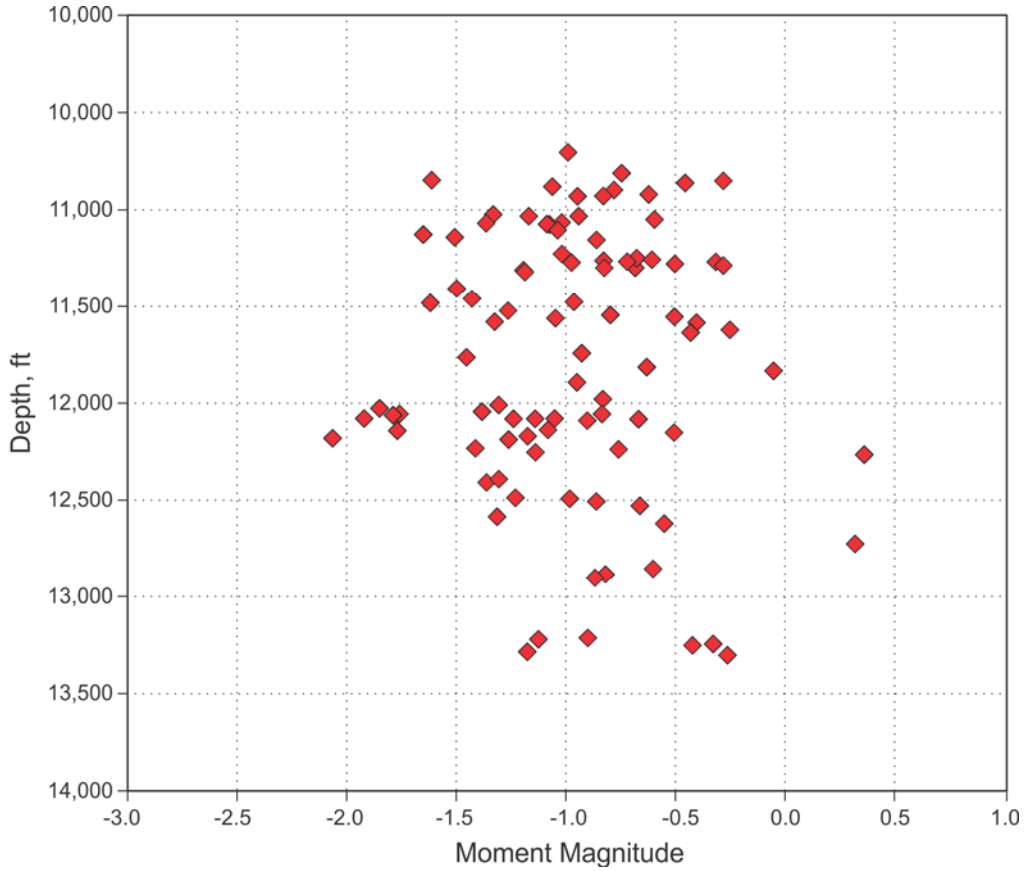

Fig. 5—Haynesville maximum moment magnitude results for monitored stages through mid 2011.

The Horn River basin in northeast British Columbia has several shale reservoirs that are targets for production, including the Muskwa, Evie, and Keg River. The results for those reservoirs are shown in **Fig. 6** as a function of depth. The stair-step nature of the results is most likely because there is only a limited amount of information available. The largest events are on the order of +1.0 M_w, and these occur in the deeper parts of the basin.

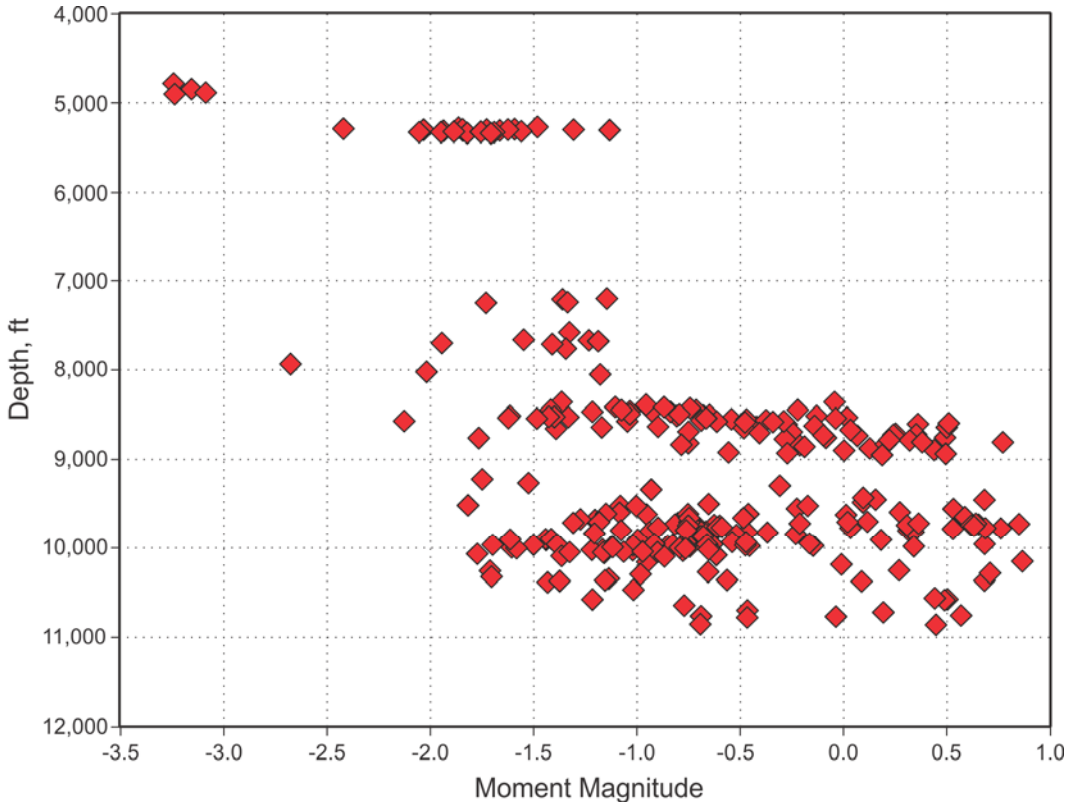

Fig. 6—Muskwa/Evie reservoir maximum moment magnitude results for monitored stages through mid 2011.

Effect of Rate and Volume

Although there is some concern about the high injection rates and large volumes pumped into these shale reservoirs, the results of the microseismic monitoring show no evidence of either rate or volume effects on the size of the microseisms. **Fig. 7** shows a plot of moment magnitude versus average rate, and **Fig. 8** shows a plot versus injected volume for the Barnett shale, the most comprehensive data set. It should be noted that rate and volume information are not nearly as reliable because of the various aspects of the reporting process, and only about 80% of the projects in the Barnett shale had a reliable reported injection rate, resulting in some missing data compared to Fig. 1. However, there is enough information to make clear conclusions about the lack of any correlation between moment magnitude and either rate or volume. The largest magnitude events occur at relatively modest rates and volumes and are probably much more related to location (both depth and location in the basin) than they are to the treatment parameters.

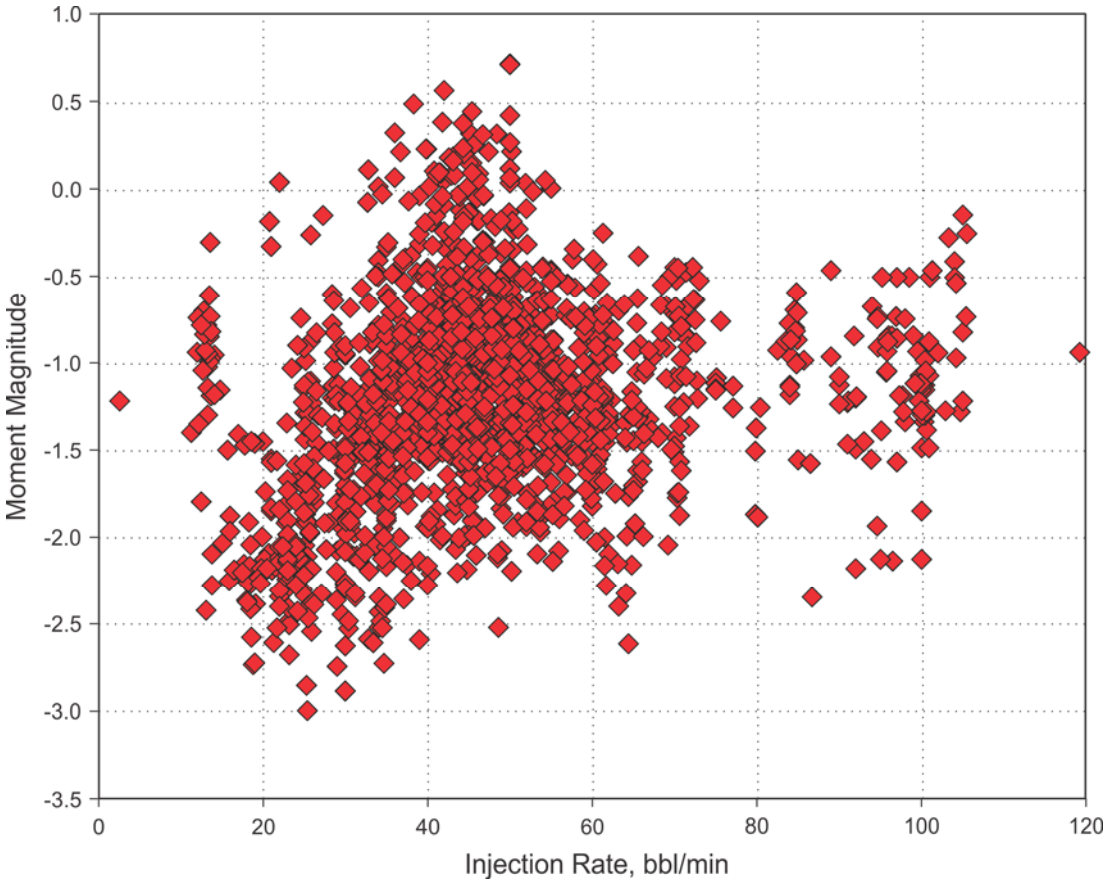

Fig. 7—Moment magnitude versus injection rate for Barnett shale projects.

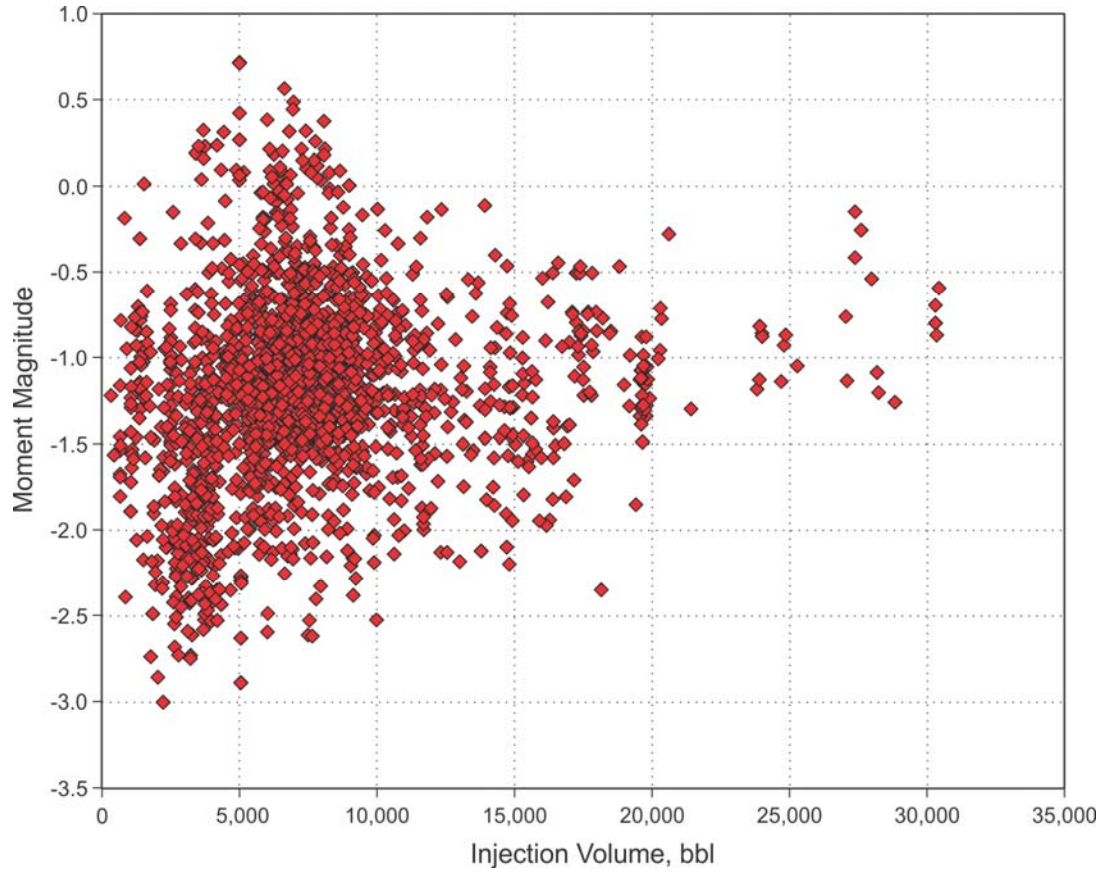

Fig. 8—Moment magnitude versus injected volume for Barnett shale projects.

Most of the other basins show similar behavior, with no clear trend with either rate or volume. The only one with even the slightest hint of any dependence is the Marcellus shale, as shown in **Fig. 9.** However, there is no indication of any volume dependence, as shown in **Fig. 10.**

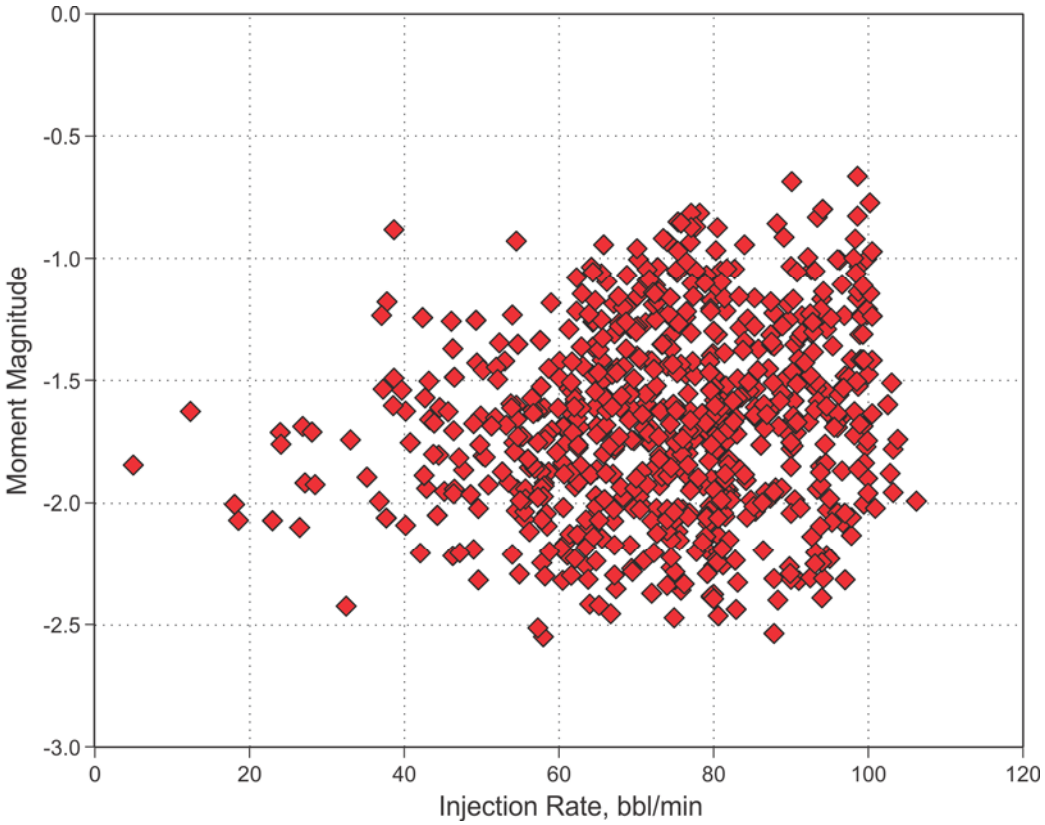

Fig. 9—Moment magnitude versus injection rate for Marcellus shale projects.

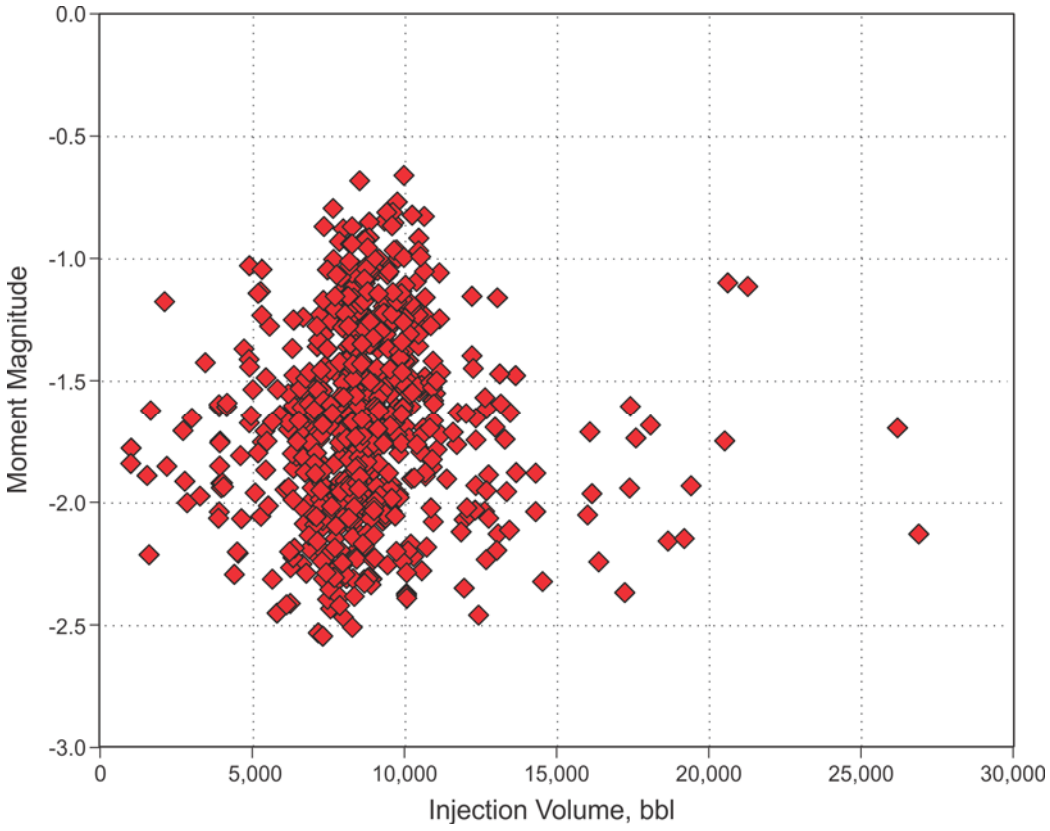

Fig. 10—Moment magnitude versus injected volume for Marcellus shale projects.

Moment and Magnitude Calculations

The analysis of the source parameters can be handled in a variety of ways. The method used here is based on the analysis by Brune (1970), where the Fourier transform of the shear-wave displacement motion can be analyzed to directly determine the seismic moment and the source radius. The equation for the moment is

$$M_o = \frac{4\pi\rho V_s^3 R\Omega_o}{F_c} \quad \text{.....(5)}$$

where ρ is the density, V_s is the shear velocity, R is the distance from the receivers to the event, Ω_o is the low-frequency amplitude of the displacement spectrum, and F_c is a radiation pattern factor.

The source dimension can be estimated by determining the corner frequency of the displacement spectrum, which is also the center frequency of the velocity spectrum. Brune (1970) gives the equation for source radius as

$$r_o = \frac{K_c V_s}{2\pi f_c} \quad \text{.....(6)}$$

where K_c is a constant (~2.2), and f_c is the corner frequency. The constant K_c has been used with different values by various authors (e.g., Madariaga 1976), but the Brune value is used here because it will provide a conservative value of the size of the slippage plane.

Fig. 11 gives an example velocity discrete Fourier transform (DFT) for a microseism generated in the Barnett shale at a distance of about 1,000 ft. This spectrum has been windowed and approximately corrected for attenuation (e.g., Gibowicz et al. 1991), and it shows a center frequency in the range of 300 to 500 Hz. The Fourier transform of the displacement is shown in **Fig. 12,** along with approximate lines showing the low-frequency amplitude and the power-law decay at high frequency. The intersection of those two lines indicates the likely corner frequency, which is approximately 300 Hz in this case, and the low-frequency amplitude of a little less than 1.E-10 in.-sec.

For typical Barnett shale shear velocity (8,000 ft/sec) and density (~2.5 gm/cc), the moment is 264,000 ft-lbf, assuming F_c = 0.5, and the magnitude is -2.4 M_w. In all cases, F_c has been assumed to be a constant, with the understanding that some microseisms will be underestimated and some overestimated. While this assumption can result in individual microseisms

being underestimated, the large population of microseisms in every fracture (and certainly throughout an entire basin) makes it unlikely that the overall maximum-magnitude result will be skewed.

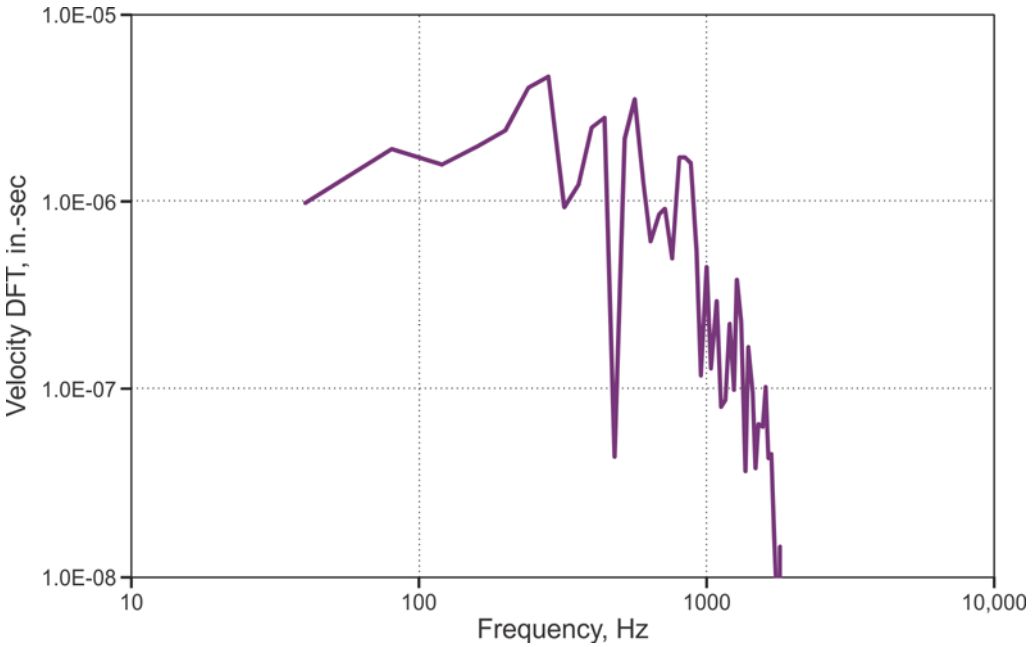

Fig. 11—Example velocity DFT for a Barnett shale shear-wave arrival.

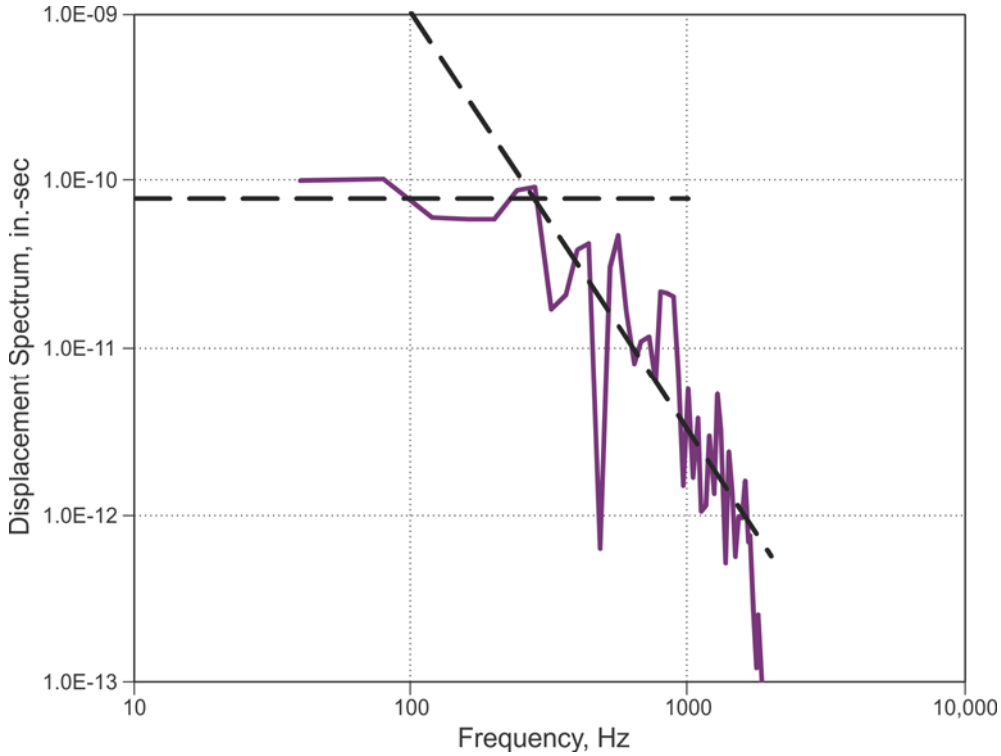

Fig. 12—Example displacement Fourier transform for a Barnett shale shear-wave arrival.

To adequately capture these spectral results, the downhole receivers used in microseismic systems must have an adequate frequency response, minimal tool resonances, and sufficient sensor response. Most of these results were captured with tool systems using fiber-optic wirelines that allowed for 1/4 msec sampling (2,000 Hz Nyquist); a small percentage were captured with tools run on standard seven-conductor wirelines that had sampling rates of 3/8 to 1/2 msec, which is still adequate sampling for the general microseisms typically observed. As can be gleaned from Figs. 11 and 12, any tool resonances are relatively small and do not interfere with attempts to capture the spectral response. The geophone sensors used have a minor mechanical mode at around 300 Hz but generally have flat response from 20 to 1200 Hz. Corrections of the acquired data for

attenuation are typically made, but these have a minimal effect on both the corner frequency and the low-frequency amplitude of the displacement. The effects of attenuation, which are principally at the higher frequencies and the farthest events, are much more severe on the slope of the falloff above the corner, but the falloff is not used here.

Much of the data from older fracture treatments had the magnitudes estimated from a correlation built for the Barnett shale. This correlation has been found to be a little low in most of the shale plays, so those results were corrected by developing a correlation between the Brune magnitude calculated above and the correlation result. Regressions were performed on many hundreds of events for each basin separately, and the older correlation data was revised accordingly. All of the data shown above relates to the Brune moment calculation, either directly or indirectly through the correction.

There are more sophisticated methods for determining the moment of a microseism using moment tensor inversion, but these techniques require two monitor wells to obtain the full moment tensor and high-quality data to get accurate information (Nolen-Hoeksema and Ruff 2001; Vavrycuk 2007; Warpinski and Du 2010). Such an inversion allows for the determination of all aspects of a source mechanism, including tensile opening and other non-pure-shear behavior. However, presently there is a very small data set of shale well treatments that used more than one monitor well. **Fig. 13** shows a comparison of the Brune magnitude with the magnitude calculated from the maximum eigenvalue of the deviatoric moment tensor for individual events in four projects with multiple monitor wells. The deviatoric moment tensor does not include any isotropic behavior—that is, purely volumetric—and it is used because it is the shear-wave energy that is of interest here. Although there is considerable scatter, there is good agreement between the Brune spectral analysis and the moment tensor inversion. Some of the Brune magnitudes are less than the moment tensor inversion, but this is expected because the spectral analysis cannot fully take into account the radiation pattern, nor will it appropriately handle non-shear behavior. Nevertheless, the ensemble of Brune magnitudes fully captures the correct maximum values of what are presumably the true moment magnitudes.

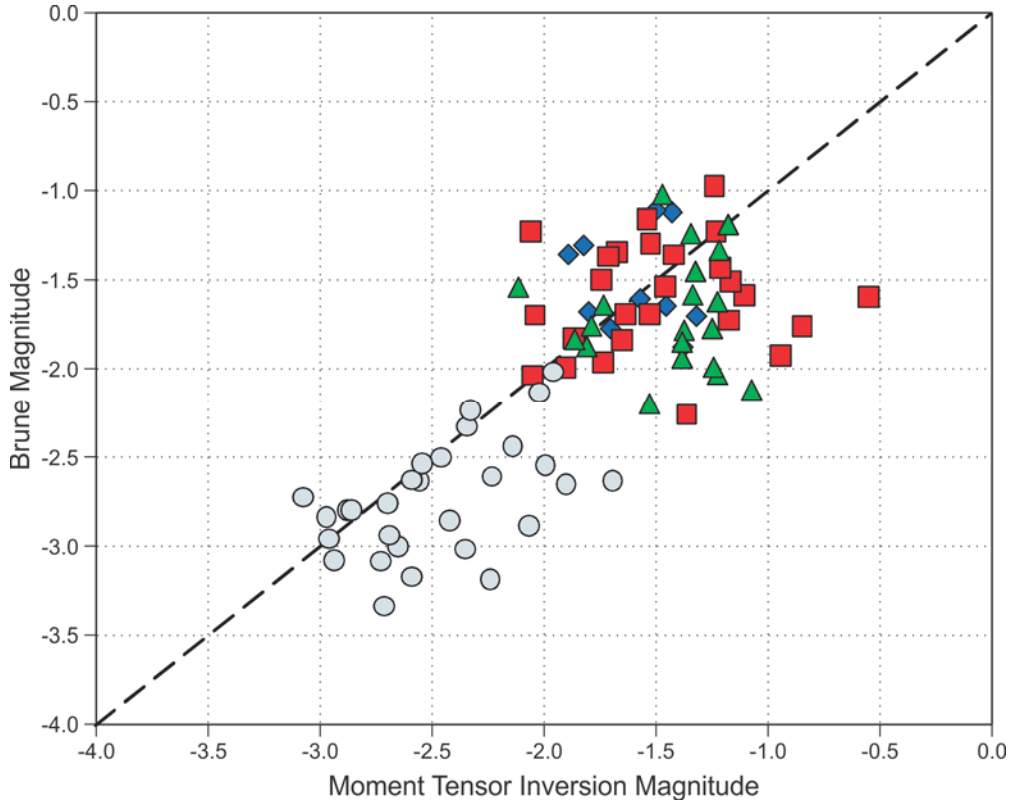

Fig. 13—Comparison of moment tensor inversion and Brune magnitudes of individual microseisms for four projects with multiple observation wells.

Practical Terms

The units associated with earthquake seismology are not intuitive, so it is helpful to relate them to specific sizes and energies. Kanamori (1977) has given a relationship for size versus magnitudes for large earthquakes, but this relationship fails for these small microseisms because it would imply extremely tiny events that would have significantly high corner frequencies, which is not what is observed. The Brune calculation of the radius can be used to generate a size-moment relationship for microseismic data. **Fig. 14** shows example data from three different shale basins, and all of them have relatively similar correlations. A regression of all of the data on a log-log plot gives

$$\log_{10}(A) = 0.988 + 0.352\log_{10}(M_o) \quad \text{.....(7)}$$

where the area is in ft^2 and the moment is in ft-lbf. It is interesting that the factor multiplying the log of the moment is much less than the 2/3 value that is expected and observed in large earthquakes, suggesting that there are significant differences in the behavior. Assuming this relationship generally holds for moment as a function of size for these fracture-generated microseisms, **Table 1** gives a suite of information about the moment, energy, area, radius, and displacement for magnitudes ranging from -4 M_w to +4 M_w. Both Fig. 14 and Table 1 are useful for understanding just how small these microearthquakes actually are.

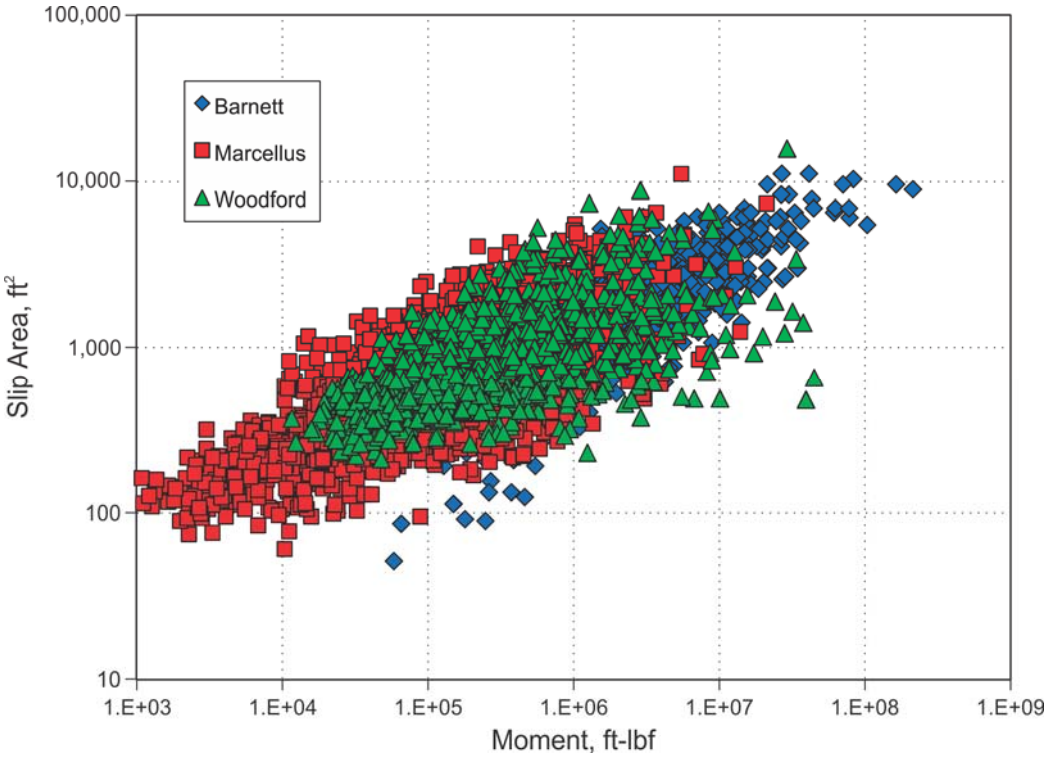

Fig. 14—Examples of relationship between microseismic slip area and moment.

TABLE 1—EXAMPLE CALCULATION OF MOMENT, ENERGY, AREA, RADIUS, AND DISPLACEMENT FOR GIVEN MOMENT MAGNITUDE MICROSEISMS

Magnitude	Moment (dyne-cm)	Moment (ft-lbf)	Energy (dyne-cm)	Energy (ft-lbf)	Radius (m)	Radius (ft)	Disp. (mm)
4	1.26e+22	9.29e+14	6.29e+17	4.65e+10	231	758	500
3	3.98e+20	2.94e+13	1.99e+16	1.47e+9	126	412	53
2	1.26e+19	9.29e+11	6.29e+14	4.65e+7	68.5	224	5.7
1	3.98e+17	2.94e+10	1.99e+13	1.47e+6	37.3	122.5	0.61
0	1.26e+16	9.29e+8	6.29e+11	4.65e+4	20.3	66.7	0.064
-1	3.98e+14	2.94e+7	1.99e+10	1.47e+3	11.1	36.3	6.9e-4
-2	1.26e+13	9.29e+5	6.29e+8	4.65e+1	6.0	19.8	7.4e-4
-3	3.98e+11	2.94e+4	1.99e+7	1.47	3.3	10.8	7.9e-5
-4	1.26e+10	9.29e+2	6.29e+5	.0465	1.8	5.9	8.4e-7

These calculations also bring up some informative data on the value of microseisms for understanding the hydraulic fracturing process. Clearly, the locations of the microseisms outline the geometry of the hydraulic fracture and provide information on the growth behavior. However, some recent analyses have suggested that the microseisms also provide information about the hydraulic fracturing growth process itself, possibly yielding information about proppant distribution, tensile fracturing, permeability enhancement, and much more. This, of course, seems to be a false hope that can be easily dismissed by examining the conditions associated with the microseismicity.

A relatively large microseism for any normal treatment in a typical shale reservoir that does not intersect a fault will typically be a -2.0 M_w. Usually, there are a few hundred identifiable microseisms in any treatment stage; but, to be conservative, assume there are 1,000 of these relatively large events. The total energy in 1,000 -2.0 M_w events would be about 46,500 ft-lbf. By contrast, the total energy injected into a typical fracturing stage may consist of a 2- to 3-hour injection using 25,000 hhp, for a total input energy of 10^{11} ft-lbf. Some of this energy is lost as friction and leakoff, but a shale formation biwing fracture with common dimensions of 2,000-ft wing length and 300 ft of height with a 5-mm opening pumped at 8,000-psi bottomhole pressure would have useful work of about 2×10^{10} ft-lbf. This is about 20% of the total energy input and probably a low estimate (i.e., there likely are more fractures or larger fractures), but it is clearly in a reasonable maximum range and shows how much energy may go into creating and enlarging the tensile fracture. When compared to the seismic energy released—on the order of a million times greater—it is clearly implied that a hydraulic fracture is largely aseismic, as suggested by Maxwell (2011), using pressure spectra as supporting evidence.

In fact, the pressure analysis suggested by Maxwell (2011) is somewhat indirect, but downhole tiltmeter data has been used to actually measure the deformation associated with a growing hydraulic fracture, and a similar analysis can be performed directly on the measured deformation. **Fig. 15** shows a spectrum of the tiltmeter measured deformation that occurred in a hydraulic-fracture treatment at the M-Site experiment in the Piceance basin of Colorado (Branagan et al. 1996; Warpinski et al. 1997). This test had both downhole microseismic receivers and downhole tiltmeters cemented into a closely spaced offset wellbore, and the tiltmeter data were inverted to extract the growth of the fracture as a function of time. The result is a deformation measurement in the reservoir at the location of the monitor well, which reflects the actual opening behavior of the fracture. The spectrum is similar to that presented by Maxwell (2011) for pressure, and clearly shows that all of the deformation is occurring at frequencies that are orders of magnitude lower than the seismic range. Clearly, anything observed in the seismic range is an inconsequential feature of the stress and pressure inflicted on the reservoir and tells nothing of value about the process. Luckily, the locations of the microseisms are of value, and they do mark out the general fracture shape, growth, and behavior.

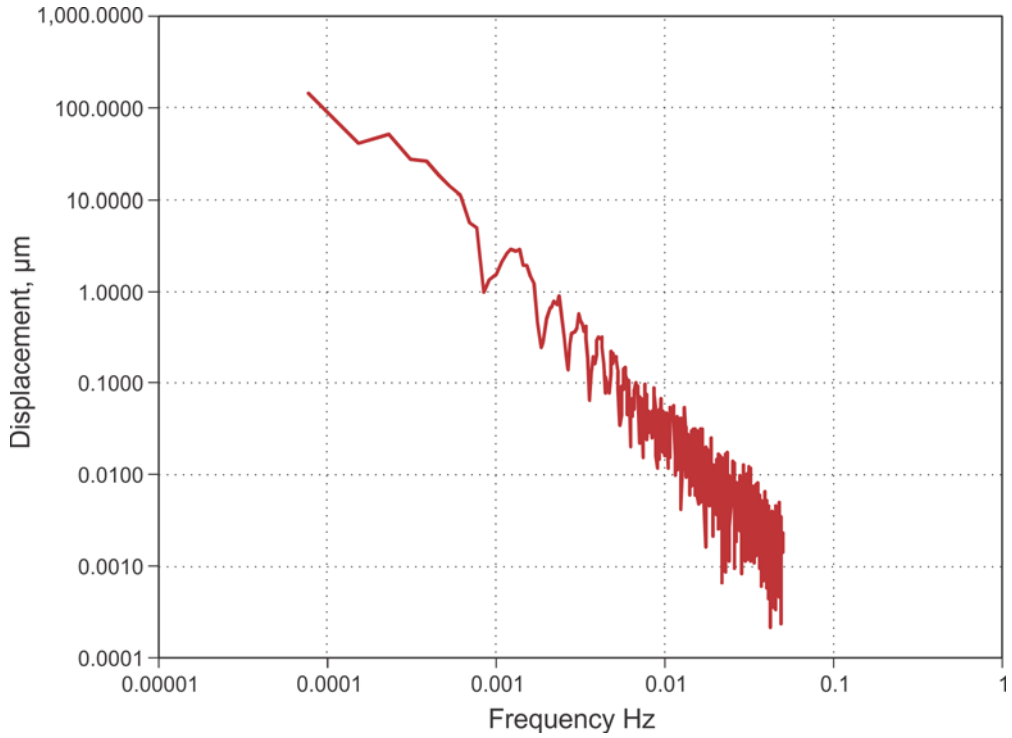

Fig. 15—Displacement spectrum measured using downhole tiltmeters at an observation well approximately 300 ft from fracture.

Furthermore, these types of calculations can be used to show that any attempt to infer the stimulated reservoir volume (SRV) from microseismic source analyses is also a gross error. While the locations of the microseismic activity clearly show the SRV, the source data are meaningless. Assume again that there are1,000 -2.0 M_w events and also that the average corner frequency is 200 Hz (this can actually be relaxed). A 200-Hz corner frequency implies a radius of 11 ft (3.4 m) from the Brune analysis and an area of 380 ft^2 (36 m^2). The amount it actually slips can then be calculated from the moment, by means of $M_o = \mu A d$, where μ is the shear modulus, A is the area, and d is the slip. For a typical shale, μ will be on the order of 2.2×10^6 psi (15 GPa), giving a slippage of 0.00009 in. (0.002 mm). If it is assumed that half of that slippage is opening (which actually seems overly large), then the volumetric increase caused by the microseism is the area multiplied by the opening slippage, or 0.0014 ft^3. With 1,000 microseisms, there would be 1.4 ft^3, or about 0.25 bbl. Because a typical treatment injects 10,000 to 20,000 bbl, it is impossible to see how the microseismic source behavior that might reflect only 1/1,000th of a

percent of the injected volume will somehow provide information on how the fracture is behaving, or how the SRV is growing. Note that changing the corner frequency does not help because the product of A and d is only dependent on the moment and the shear modulus. Only a lower shear modulus or a larger moment would increase the volume significantly.

Observation Distance

To make important deductions about the behavior of hydraulic-fracturing treatments in shales, it must first be possible to image all the important elements of the fracture. It is fortunate that the microseismic activity in shale reservoirs is large enough to be observed long distances with the sensitive receiver systems that are now available (Note: This is not the case for some other hydrocarbon reservoirs).

One means of determining the ability to view microseisms in any test is to plot the measured moment magnitude as a function of distance from the observation well. An example of such a plot is shown in **Fig. 16** for tests conducted in four different shale basins. The results are typical of what is observed in these tests, except that they were selected for inclusion here because they all have relatively large microseisms. One can usually draw a line along the bottom of the distribution of the microseisms, and this line is clearly a viewing-limit line. Larger events can be observed at greater distances, while small events must be close to the observation well. This type of plot is useful for many quality-control applications; but here, the primary interest is to illustrate how far these microseisms can be detected.

While a typical event is -2.5 M_w, which can be observed 3,000 ft away, larger events that are clearly the important ones can be detected and located at distances of 4,000 ft and greater. By extrapolation, the viewing limit line suggests that large magnitude events can be detected at even greater distances, potentially a few miles if events were extremely large. It should also be noted that the distance in Fig. 16 is the lateral distance from the monitoring wellbore, and the layering found in these shale basins may reduce the viewing distance somewhat. However, this data set contains many monitoring tests where the receivers were many hundreds of feet above the microseisms, with little effect on the viewing distance. In addition, fractures seldom grow very far vertically from the interval that is being treated (Fisher and Warpinski 2011), so the likelihood of needing to detect microseisms across a large number of layers is limited.

This ability to detect microseisms at great distances makes the mapping useful and clearly shows that this technology can normally detect the farthest significant microseisms.

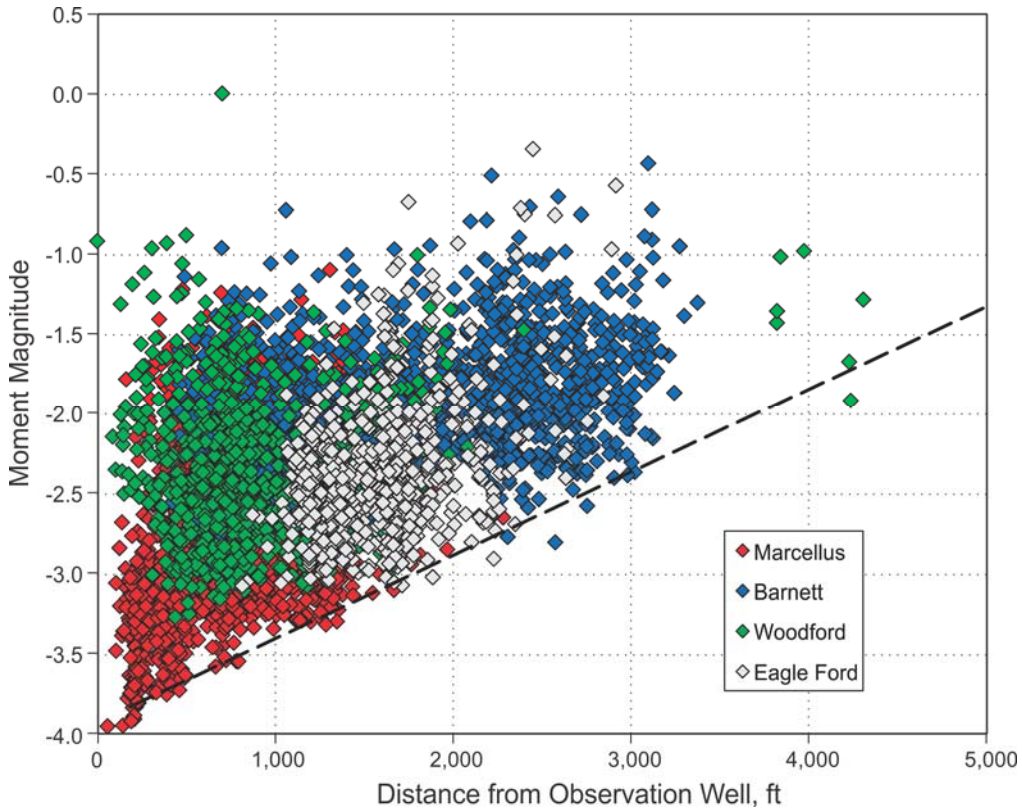

Fig. 16—Moment magnitude vs. distance plot for several shale treatments in different basins.

Discussion

Hydraulic fracturing is a critical technology for economically extracting natural gas from ultralow-permeability shale reservoirs, but it is also important that the environment be protected in any extraction endeavor. Microseismic results from

several thousand fracture treatment stages in shale reservoirs were assembled to investigate the possibility of detrimental consequences from induced seismicity in these reservoirs. For all of the data the authors have reviewed to date, there is no evidence of any harmful occurrence as a result of the treatments conducted in these reservoirs. The moment magnitudes of the earthquakes are a few magnitude units lower than anything that might cause problems, and the corresponding energies are many orders of magnitude lower. These microseisms have minute slippages happening over relatively small areas (on the order of the size of the reservoir or smaller).

The microseismicity generally shows an increase in magnitude with depth, suggesting that some combination of the higher pressures and the larger in situ stresses at depth result in a larger energy release. In some cases, such as the Woodford shale, the relationship between magnitude and depth is dramatic. The difference between shallow and deep microseismic magnitudes can be 2.5 to 3.0 magnitude units. Others, such as the Marcellus shale, do not exhibit much depth dependence.

One interesting result is the lack of any significant variation of the magnitudes with either injection rate or injection volume. Some of this insensitivity might be more a result of the distribution of rates and volumes. Most treatments tend to be conducted within a fairly narrow range for most of these basins. A much smaller number of treatments have typically been conducted differently as a result of early trial and error, problems during a treatment, experimentation in outlying areas, or other non-recurring factors. If the larger microseisms occur as a result of fault interaction, then the rates and volumes at which most of the treatments are conducted are most likely to be the conditions under which the faults would be encountered and the largest microseisms be generated. On the other hand, if microseismic activity is primarily a function of the treatment conditions (i.e., rate and/or volume), then there should be a clear relationship, even if there are limited results at higher rates and larger volumes. These data suggest that the induced seismicity is not a function of treatment conditions, but rather of the fault interactions caused by geologic/structural/stress conditions in the reservoir. This is an important result because it implies that induced seismicity can be minimized by avoiding fracturing in structurally complex areas, or at least carefully monitoring any stimulation activities that occur.

In practical terms, the typical largest microseism in normal fracture treatments is a -2.5 M_w. Using Table 1, a microseism of this size would have a slip radius of around 20 ft and a minute displacement on the order of the grain size. This size microseism does not even extend across the full height of the reservoir for a typical shale environment. For the largest observed microseism (M_w < 1.0), the radius is on the order of 100 ft and the slip is on the order of one-half millimeter. This size is on the order of the thickness of the reservoir. As indicated by the height data presented in Fisher (2010) and Fisher and Warpinski (2011), this activity occurs extremely close to the reservoir depth.

The microseisms generated by hydraulic fracturing in these shales show a similar behavior for estimated slip area as a function of magnitude in the various basins. These two properties are calculated using extremely different properties of the waveform. The size is based on the corner frequency of the displacement spectrum, while the moment (from which the moment magnitude is derived) is based on the low-frequency amplitude of the displacement spectrum. There is no reason computationally why these parameters should be related (i.e., it is not an artifact of the processing), so this observation is presumably a reflection of the intrinsic behavior of microseismicity in shale reservoirs. The size magnitude is significantly different from that observed in large earthquakes (Kanamori 1977), but that is not surprising given the different energy, stress, size, and shear conditions.

The small size of the microseisms observed in these treatments puts a limit on the value of the microseismic characteristics for interrogating the fracturing process. Clearly, the microseisms reflect effects resulting from the presence of the fracturing fluid injection, and thus if we can detect and locate them, they provide a means for increased understanding of the geometry of the growing hydraulic fracture, or especially in many shale reservoirs, the fracture network being created and enlarged. Because these shales are undersaturated with respect to water, and the minute pore spaces of the rock matrix will have large capillary pressures, it is a given that any natural fractures or other discontinuities in the reservoir will be gas-filled (or closed/rehealed). Destabilization of the reservoir that would be responsible for the concurrent microseismicity can only occur with leakoff of the high-pressure fracturing fluid (Warpinski et al. 2004). This is primarily because any dilating fracture generates solid stresses that are stabilizing and shear-reducing, where a greater stress change is added in the minimum in-situ stress direction, thus reducing the shear and, at the same time, increasing the normal stress on any plane. The end result is that the microseismic locations must be located close to the hydraulic fracture (or fracture network) where leakoff can occur into natural fractures or other features, except for the region around the fracture tip where large shear stresses can be generated and the net stress is reduced because of the tensile "jacking-open" of the formation ahead of the fracture. This is a fortunate occurrence, and it is the principal reason why microseismic mapping can provide significant value in revealing the fracture geometry and behavior.

On the other hand, the energy in the microseismicity is minute compared to the energy that is necessary to create and grow the fracture; so, any inference about the fracture opening process by detailed examination of the microseisms is clearly flawed. Such inferences would be about some aspect of the rock behavior reflecting roughly one millionth of the energy input. The bulk of the deformation associated with the fracture process (width growth) is clearly aseismic and cannot be inferred from the limited microseismicity that occurs. The promise of moment tensor inversion and other source analyses is in the potential for reservoir characterization (natural fracture planes and stress), not in the type of fracturing that is occurring.

The same analysis can be conducted with respect to the size of the microseismic volume relative to the SRV. This volume is so small relative to the injected volume that it obviously is not a reflection of the fracture or network volume that is created. This fact should be obvious to anyone examining these fractures; the reservoir is extremely low-permeability and

little fluid is lost into the matrix during fracturing. The fluid must create one or more hydraulic fractures and also leakoff into, extend, and/or dilate existing natural fractures, either open or rehealed ones. The "microseismic source volume" is inconsequential, and it should not be confused with the microseismic fracture volume as reflected in either fracture geometry or network volume (SRV).

In summary, microseismicity is an incredibly useful feature that comes for free with hydraulic fracturing. It maps out the fracture, but is relatively small and not harmful in any normal circumstances. It reveals much about the fracture geometry and the way the fracture evolves but does not provide detailed information about the fracturing process, other than what can be gleaned from the locations. The additional promise is in the possibility of enhanced reservoir characterization, although this aspect has been of only limited value to date.

Conclusions

Microseismicity has been monitored in thousands of fracture treatments in all of the major shale basins in North America and has been observed to be extremely small in magnitude, energy, and size. Typical microseisms are less than -2.5 M_w, and average microseisms are approximately -3.0 M_w in these reservoirs. The largest monitored microseisms within the authors' database are less than 1.0 M_w, which is much smaller and less energetic than any event that would be damaging or harmful.

The observed microseismicity is similar from basin to basin for the formations reviewed here, with some differences that probably result from depth, structure, and other geologic differences. There is a general decrease in magnitude, energy, and size with decreasing depth, such that the shallowest microseisms are generally the smallest. Rate and volume do not appear to have much effect on the observed microseismicity, at least within the limits of typical fracturing conditions in these basins.

Microseismicity is a useful tool, but it is sometimes overinterpreted in attempts to yield additional information about the fracture(s). The size of these events reflects a minute fraction of the input energy and volume, and any attempt to use various types of source information to understand the fracture process other than location is unsupportable.

Acknowledgements

The authors thank Halliburton for permission to publish this paper. In addition, they acknowledge the hard work of many geophysicists, engineers, and field crews who have acquired and processed these data.

Nomenclature

A = area of slippage zone, L^2, ft^2 [m^2]
d = slippage distance, L, ft [m]
E = seimic energy, ML/S^2, ft-lbf [joule]
f_c = corner frequency, 1/S, Hz
F_c = radiation pattern factor
K_c = slippage radius factor
M_o = seismic moment, ML/S^2, ft-lb [N-m]
M_w = moment magnitude
r_o = fault radius, L, ft [m]
R = distance from observation point to slippage, L, ft [m]
V_s = shear-wave velocity, L/S, ft/sec [m/sec]
μ = shear modulus of rock, M/LS^2, psi, [MPa]
ρ = rock density, M/L^3, lbm/ft^3 [kg/m^3]
Ω_o = low-frequency, shear-wave amplitude of displacement Fourier transorm, L-S, ft-sec [m-s]

References

Ake, J., Mahrer, K., O'Connell, D.O., and Block, L. 2005. Deep-Injection and Closely Monitored Induced Seismicity at Paradox Valley, Colorado. *Bulletin of the Seismological Society of America* **95** (2): 664–683.

Aki, K. and Richard, P.G. 2009. *Quantitative Seismology, 2nd Edition*. University Science Books. Sausalito, California.

Branagan, P.T., Warpinski, N.R., Engler, B.P., Wilmer, R. 1996 Measuring the Hydraulic Fracture-Induced Deformation of Reservoir and Adjacent Rocks Employing a Deeply Buried Inclinometer Array: GRI/DOE Multi-Site Project. Paper SPE 36451 presented at the SPE Annual Technical Conference and Exhibition, Denver, Colorado, USA, 6–9 October. doi: 10.2118/36451-MS.

Brune, J.N. 1970. Tectonic Stress and the Spectra of Seismic Shear Waves from Earthquakes. *Journal of Geophysical Research* **75** (26): 4997–5009.

Duda, J.R., Boyer, C.M., Delozier, D., Merriam, G.R., Frantz, J.H., and Zuber, M.D. 2002. Hydraulic Fracturing: The Forgotten Key to Natural Gas Supply. Paper SPE 75712 presented at the SPE Gas Technology Symposium, Calgary, Alberta, Canada, 30 April–2 May. doi: 10.2118/75712-MS.

Fast, C.R., Holman, G.B., and Covlin, R.J. 1977. The Application of Massive Hydraulic Fracturing to the Tight Muddy "J" Formation, Wattenberg Field, Colorado. *J. Pet. Tech.* **29** (1): 10–16.

Fehler, M.C. 1989. Stress Control of Seismicity Patterns Observed during Hydraulic Fracture Experiments at the Fenton Hill Hot Dry Rock Geothermal Energy Site, New Mexico. *International Journal of Rock Mechanics, Mining Sciences, and Geochemical Abstracts* **26** (3–4): 211–219.

Fisher, M.K. 2010. Data Confirm Safety of Well Fracturing. *The American Oil & Gas Reporter*. July.

Fisher, M.K. and Warpinski, N.R. 2011. Hydraulic Fracture Height Growth: Real Data. Paper SPE 145949 presented at the SPE Annual Technical Conference and Exhibition, Denver, Colorado, USA, 30 October–2 November. doi: 10.2118/145949-MS.

Gibowicz, S.J., Young, R.P., Talebi, S., and Rawlence, D.J. 1991. Source Parametes of Seismic Events at the Underground Research Laboratory in Manitoba, Canada: Scaling Relations for Events with Moment Magnitude Smaller than -2. *Bulletin of the Seismological Society of America* **81** (4): 1157–1182.

Gidley, J.L., Mutti, D.H., Nierode, D.E., Kehn, D.M., and Muecke, T.W. 1979. Stimulation of Low-Permeability Gas Formations by Massive Hydraulic Fracturing–A Study of Well Performance. *J. Pet. Tech.* **31** (4): 525–531.

Jennings, A., Darden, W., Wenzel, R., Shrat, R. and Foster, J. 1977. Massive Hydraulic Fractures in the Eastern United States. Paper SPE 6866 presented at the SPE Annual Technical Conference and Exhibition. Denver, Colorado, USA, 9–12 October. doi: 10.2118/6866-MS.

Kanamori, H. 1977. The Energy Release in Great Earthquakes. *Journal of Geophysical Research* **82** (20): 2981–2987.

Madariaga, R. 1976. Dynamics of an Expanding Circular Fault. *Bulletin of the Seismological Society of America* **66** (3): 639–666.

Maxwell, S.C. 2011. What Microseismic Does and Does Not Indicate about Hydraulic Fractures. Paper presented at the 73rd EAGE Conference and Exhibition incorporating SPE EUROPEC 2011, Vienna, Austria, 23–26 May.

Montgomery, C.T. and Smith, M.B. 2010. Hydraulic Fracturing: History of an Enduring Technology. *J. Pet. Tech.* **62** (12): 26–32.

Nicholson, C. and Wesson, R.L. 1990. Earthquake Hazard Associated with Deep Well Injection–A Report to the U.S. Environmental Protection Agency. U.S. Geological Survey Bulletin 1951. Denver, Colorado.

Nolen-Hoeksema, R.C. and Ruff, L.J. 2001. Moment tensor inversion of microseisms from the B-sand propped hydrofracture, M-site, Colorado. *Tectonophysics* **336** (1–2): 163–181.

Overby, W.K. 1978. Present Status of the Eastern Gas Shales Project. *METC/SP-78/6, Second Eastern Gas Shales Symposium Volume 2*, US Dept. of Commerce: Morgantown, West Virginia.

Segall, P. 1989. Earthquakes Triggered by Fluid Extraction. *Geology* **17** (10): 942–946.

Smith, W., Beall, J. and Stark, M. 2000. Induced Seismicity in the SE Geysers Field, California, USA. Proceedings of the World Geothermal Congress. Kyushu-Tohoku, Japan, 28 May–10 June.

Strubhar, M.K., Fitch, J.L., and Medlin, W.L. 1980. Demonstration of Massive Hydraulic Fracturing, Piceance Basin, Colorado. Paper SPE 9336 presented at the SPE Annual Technical Conference and Exhibition, Dallas, Texas, USA, 21–24 September. doi: 10.2118/9336-MS.

Sutton, R.P., Cox, S.A., and Barree, R.D. 2010. Shale Gas Plays: A Performance Perspective. Paper SPE 138447 presented at the SPE Tight Gas Completions Conference, San Antonio, Texas, USA, 2–3 November. doi: 10.2118/138447-MS.

Vavryčuk, V. 2007. On the retrieval of moment tensors from borehole data. *Geophysical Prospecting* **55** (3): 381–391.

Warpinski, N.R., Branagan, P.T., Engler, B.P., Wilmer, R., and Wolhart, S.L. 1997. Evaluation of a Downhole Tiltmeter Array for Monitoring Hydraulic Fractures. *International Journal of Rock Mechanics and Mining Sciences* **34** (4): 108.e1-108.e13.

Warpinski, N.R., Wolhart, S.L., and Wright, C.A. 2004. Analysis and Prediction of Microseismicity Induced by Hydraulic Fracturing. *SPE Journal* **9** (1): 24–33.

Warpinski, N. 2009. Microseismic Monitoring: Inside and Out. *J. Pet. Tech* **61** (11): 80–85. SPE- 118537-MS. doi: 10.2118/118537-MS.

Warpinski, N.R. and Du, J. 2010. Source-Mechanism Studies on Microseismicity Induced by Hydraulic Fracturing. Paper SPE 135254 presented at the SPE Annual Technical Conference and Exhibition. Florence, Italy, 19–22 September. doi: 10.2118/135254-MS.

Zoback, M.D. and Harjes, H.P. 1997. Injection-Induced Earthquakes and Crustal Stress at 9 km Depth at the KTB Deep Drilling Site, Germany. *Journal of Geophysical Research*. **102** (B8): 18,477–18,491.